Modeling HF Gain Generator F-Atom Flows

10 May 2003

Prepared by

M. A. KWOK and S. T. AMIMOTO
Space-Based Laser
Space Support Division

Prepared for

SPACE AND MISSILE SYSTEMS CENTER
AIR FORCE SPACE COMMAND
2430 E. El Segundo Boulevard
Los Angeles Air Force Base, CA 90245

Space Systems Group

1/Lt William Welser IV
SMC/MTZ

REPORT DOCUMENTATION PAGE

1. REPORT DATE (DD-MM-YYYY)	2. REPORT TYPE	3. DATES COVERED (From - To)
10-05-2003		

4. TITLE AND SUBTITLE	5a. CONTRACT NUMBER
Modeling HF Gain Generator F-Atom Flows	F04701-00-C-0009
	5b. GRANT NUMBER
	5c. PROGRAM ELEMENT NUMBER

6. AUTHOR(S)	5d. PROJECT NUMBER
Munson A. Kwok and Sherwin T. Amimoto	5e. TASK NUMBER
	5f. WORK UNIT NUMBER

7. PERFORMING ORGANIZATION NAME(S) AND ADDRESS(ES)	8. PERFORMING ORGANIZATION REPORT NUMBER
The Aerospace Corporation Space Support Division El Segundo, CA 90245-4691	TR-2000(1019)-1

9. SPONSORING / MONITORING AGENCY NAME(S) AND ADDRESS(ES)	10. SPONSOR/MONITOR'S ACRONYM(S)
Space and Missile Systems Center Air Force Space Command 2430 E. El Segundo Blvd. Los Angeles Air Force Base, CA 90245	SMC
	11. SPONSOR/MONITOR'S REPORT NUMBER(S)
	SMC-TR-03-23

12. DISTRIBUTION/AVAILABILITY STATEMENT

Approved for public release; distribution unlimited.

13. SUPPLEMENTARY NOTES

14. ABSTRACT

Control volume analysis and one-dimensional reacting gasdynamics have been combined with a unique thermal-mechanical model of a combustor vessel to estimate production of fluorine atoms at the nozzle exit plane. Upon reaction with hydrogen, H_2, these F-atoms are a key species in the efficient production of internally energetic hydrogen fluoride (HF) molecules, which is the lasant material for an HF chemical laser. Thus, a quantitative estimate of F-Atom density and more specifically the degree of fluorine (F_2) dissociation, α, is an essential parameter for the accurate prediction of laser performance. This parameter, as a function of time, has been difficult to experimentally measure or to analyze in such lasers.

The method has been applied to the only cylindrical HF chemical laser in operation. Test conditions for the most recent tests of the Alpha Laser are analyzed. It is found for the baseline operating point that α reaches a plateau exceeding 0.9 after a sufficiently long operating time. Necessarily for the expediency of rapid calculations, such a model lacks the temporal and spatial fine details of the heat transfer processes, gasdynamics, and boundaries. Therefore, such a model is valuable for insight, but must be used with care for detailed design.

15. SUBJECT TERMS

Chemical lasers, HF lasers, Space-based lasers, High-power lasers, Combustors, Combustor models, Gain generators, Reactive flow

16. SECURITY CLASSIFICATION OF:			17. LIMITATION OF ABSTRACT	18. NUMBER OF PAGES	19a. NAME OF RESPONSIBLE PERSON Munson Kwok
a. REPORT	b. ABSTRACT	c. THIS PAGE		33	19b. TELEPHONE NUMBER (include area code)
UNCLASSIFIED	UNCLASSIFIED	UNCLASSIFIED			(310)336-5441

Acknowledgments

Contents

Figures

Tables

1. Introduction

The cylindrical or annular HF chemical laser known as the Alpha Laser has been previously described.[1] In this report, we will concentrate on the gain generator part of the system, which produces the F-atom radicals necessary for the production of the lasant, HF*, namely, HF with inverted vibrational and rotational state distributions. The HF* is produced by the chemical reaction

$$F + H_2 \longrightarrow HF + H, -\Delta H = 31.6 \text{ kcal/moles} \qquad (1)$$

The gain generator is the cylindrical vessel containing the combustor or plenum generating the F-atoms from a hot, chemically reacting mixture at a steady stagnation temperature approaching 2000K. The hot gases are exhausted from the plenum through an annular nozzle array serving as the cylindrical walls of the plenum, in an essentially azimuthally uniform radial flow. The nozzles in the array are a converging-diverging type to generate a supersonic jet exhaust into a good background vacuum. The trailing edges of aerodynamic blades at the nozzle exit planes inject cold hydrogen into the hot stream. The gain medium is formed by free jet mixing with the hydrogen. The annular gain medium is approximately 50 cm in radius with a width or "thickness" of 2.5–3.5 cm. An annular resonator structure, the HEXDARR (High EXtraction Efficiency Decentered Annular Ring Resonator), extracts laser power from this medium over a length of approximately 400 cm in a double pass. It is apparent from Eq. (1) that laser power performance will be strongly proportional to the F-atom flow out of the nozzle exit planes, but it will depend somewhat on the plenum stagnation temperature, reaction kinetics, and the degree of F_2 dissociation at that plane. The plenum temperature depends sensitively on the combustion process, as we will see, and it determines to a great extent the F-atom production and also the static temperature in the free jet. Both gas properties affect the small signal gain coefficients of each spectral line in the flow direction. Laser power performance will also be affected by the presence of small amounts of F_2 created by recombination in the plenum and in the nozzle arrays when the plenum temperature is not high enough. In this case, the free H-atom generated by Eq. (1) can react with F_2 in the so-called "hot reaction" of the chain to raise significantly the static temperature of the free jet, effectively lowering small signal gains and even shortening the annular gain width by enhancing quenching collision kinetics. The $H + F_2$ reaction has an exoergicity of 91 kcal/mole, almost 3 times that of Eq. (1). Unfortunately, in contrast to Eq. (1), little of this large heat release leads to productive HF* gain for lasing.

Thus, a major goal of gain generator design has been to minimize the presence of F_2 in the free jet. This challenge is difficult to meet because space laser requirements virtually dictate a regeneratively cooled plenum of low mass content. Yet, the complex structure is of sufficient size that practical laser operation occurs in a transient thermal and mechanical condition, which is difficult to model. The empirical Alpha Laser experience has been essential for understanding any future design approaches.

A simple model for predicting F_2 degree of dissociation is sought to guide conceptual design or test planning. In this work, we propose to develop a simple, spreadsheet combustor model that focuses on predicting F-atom production across the nozzle exit planes. Our objective is to provide sufficient insight to help understand observed laser performance data on a device such as the Alpha Laser and also to help in developing combustor operating points for future laser devices. Our approach is the classical application of Control Volume analysis to describe the combustor process.[2] The advantage of this method is that the practitioner defines the boundary of study to eliminate much of the structural and reactive flow intricacies. Once the Control Volume is defined, analysis must be developed for transient nozzle throat changes due to thermal effects and their linkages to combustor plenum pressure changes. The quantitative development of this linkage is the one unique aspect of this report. In such an approach, one deliberately sacrifices the spatial and temporal details that might influence an actual differential fluid element, in quest of averaged quantities that will reflect the global behavior of the system with acceptable fidelity.

As a demonstration of its application, the model will be used to compute the F_2 degree of dissociation, α, as a function of time for two tests with essentially the same flow rates in steady state, namely, HL902 and HL909B. A short model uncertainty discussion will follow.

2. Model Logic

The logic for building the thermal energy flux balance for the model is as follows:

1. Estimate thermal energy flowing in with reagents during interval Δt.

2. Estimate thermochemical energy flux released from reagents, assuming complete combustion.

3. Estimate net heat flux loss from the reagents or products during Δt interval

4. Estimate heat loss from combustor gases into the rings (and end domes) from temperature growth in the rings.

   a. Determine growth in combustor pressure P_O ($\equiv P_C$) during the interval.

   b. Relate P_O growth to nozzle throat area A^* closure. (1-D gasdynamics)

   c. Relate temperature growth in ring to A^* decrease. (linear coefficient of thermal expansion)

   d. Compute net heat flux loss from gases to vessel, given vessel temperature growth.

   e. Estimate heat loss into combustor core (found negligible).

5. From NET heat flux from reagents and product gases (items 1–3), compute "stagnation" temperature T_e of the combustor plenum. (i.e., no exhaust gasdynamics).

6. Compute F-atom density and F_2 degree of dissociation, α, given T_e.

7. Slightly corrected for further recombination through the nozzle structure to exit plane (Appendix C)

The main innovation in this heat flux model is to use the mechanical changes of the combustor vessel as indicated by gasdynamics to deduce vessel temperature growth and, thereby, the net heat flux loss from the product gas, a quantity difficult to measure directly. This vessel temperature growth manifests the net heat flux to the vessel, the difference between heat loss from the product gases, and the regenerative cooling of the vessel by reagents. Since Items 1 and 2 are well known, we will concentrate on the development of Item 3 in the following sections.

It turns out that this model is applicable provided there are no mechanical changes in the vessel due solely to P_c pressure changes. We will discover later that this assumption approaches validity beyond $t \geq 8$ s in the cases discussed here when the flows reach a true steady state and combustion is well established. (See Figure 3 and discussion.) An upgraded version of this model, which accommodates the detailed, fast transient behavior of P_c and the role of the cold inner core of the vessel, is reported in References 9 and 10.

3

3. Control Volume

We assume in the time increment modeled (typically 1 s) that the flow is "steady." The combustor gas properties such as molecular weight, W, specific heat, c_p, mole fractions of species, X_i, and ratio of specific heats, γ, are definable uniform quantities within a Control Volume space. These parameters for all species can be evaluated from the given reagent flowrates and gas properties and those same parameters deduced for the product species. Completed combustion and complete consumption of the oxidizer to products is assumed. There may be combustor gas property changes in succeeding time intervals due to slow changes in the flow rates of the reagents and the observed change in combustor pressure.

The choice of combustor Control Volume is illustrated in Figure 1. We attempt to choose the volume to avoid the need for specific three-dimensional details of the combustor vessel structure, including the the heat flux into reagents during regenerative cooling of the vessel and the complex details of the actually mixing of reagents at an injector system before combustion.

The Control Volume suggests the balance equation for heat flux

$$Qdot_{out} = Qdot_{inflow} + Qdot_{thermochemical} - Qdot_{gas\ loss}, \qquad (2)$$
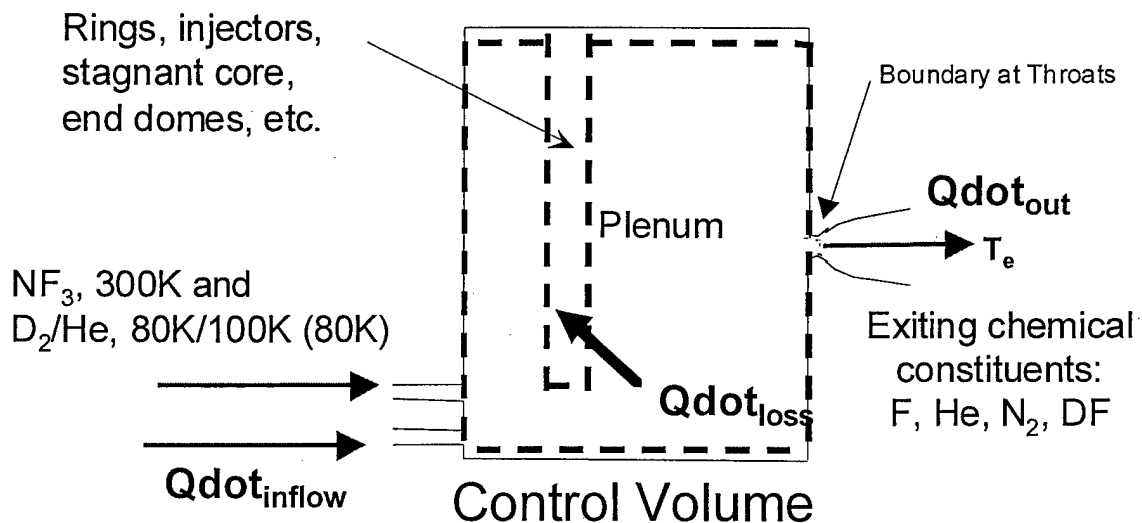
Figure 1. Illustration of the Control Volume chosen. The Control Volume is traced out by the dotted boundary, which intercepts the incoming pipes at the cryo-heat exchangers and the outflow to the nozzle throats.

where

$$Qdot_{inflow} = \sum_i [\ mdot_i c_{p-i} T_{in-i}] \tag{3}$$

With mdot, the mass flow rate, $c_p(T_{in})$, the specific heat, and T_{in}, the temperature at inflow of the ith reagent. We develop $Qdot_{thermochemical}$ and $Qdot_{loss}$ in successive sections below.

4. Thermochemistry

The combustion process begins with the early ignition by a burst of the hypergolic mixture of fluorine and deuterium. The bulk chemicals flowing into the plenum are nitrogen trifluoride, NF_3, and cryogenically cooled (to a nominal 80K) deuterium/helium mixture. In the combustion process, NF_3 readily dissociates at elevated temperature to produce F-atoms. A portion of these atoms reacts with D_2 to keep the combustor furnace going. At the plenum temperatures forecasted for the given Alpha Laser flowrates, the following chemical equation governs the process:

$$aD_2 + bNF_3 + cHe \longrightarrow 2aDF + (1/2)bN_2 + \alpha(3b-2a)F + (1-\alpha)(3b-2a)F_2 + cHe, \qquad (4)$$
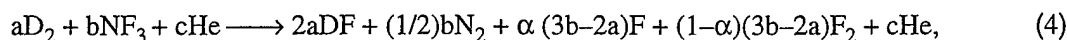
where coefficients a, b, and c are mole fractions based on incoming flow rates, and α is the degree of dissociation of molecular fluorine.

The net heat of reaction, following Eq. (4), is

$$\Delta Hnet = -a\Delta H_{D_2} - b\Delta H_{NF_3} - c\Delta H_{He} + 2a\Delta H_{DF} + 0.5b\Delta H_{N_2} + \alpha(3b-2a)\Delta H_F$$

$$+0.5(1-\alpha)(3b-2a)\Delta H_{F_2} + c\Delta H_{He} \qquad (5)$$

Of course, the heat of formation for He is moot, and those for D_2, F_2 and N_2 are zero. The heats of formation are taken at the condition of the gas crossing the Control Volume. ΔH for NF_3 is taken at 300K, and those for the combustion products, at a themochemical temperature to be defined below. A consistent solution for the combustor will, therefore, require iteration, in which gas properties are adjusted as we home in to a temperature.

We determine

$$Qdot_{thermochemical} = ndot_{in} \bullet \Delta H_{net}. \qquad (6)$$

Where $ndot_{in}$ is the total molar flowrate of reagents. We also discovered in the course of building this model the high sensitivity of the computed results to very accurate thermodynamic data of the various species. We, therefore, resorted to look-up tables based on the established JANAF database[3,4,5] and to linear interpolation between the 100K temperature intervals of the database. (Ref. 5 is probably the most useful for providing digital data and functional extrapolations.)

5. Heat Flux Loss Term

The heat flux loss from the gases is given by

$$Qdot_{loss} = Qdot_{rings} - Qdot_{struts} + Qdot_{domes} + Qdot_{stagnant\ core}, \qquad (7)$$

with

$$Qdot_{rings} = [Qdot_{convective} + Qdot_{radiative} - Qdot_{regen}] \qquad (7a)$$

$Qdot_{domes}$ will become a small multiplicative correction factor on $Qdot_{rings}$ in Eq. 16, while $Qdot_{struts}$ and $Qdot_{stagnant\ core}$ can be shown to be negligible heat conductors. Thus, evaluation of $Qdot_{loss}$ centers on a good estimate of $Qdot_{rings}$, the net heat flux gained by the rings.

In the time interval Δt of assumed "steady" flow, the total mass flow rates, individual mass flow rates, the specific heats, and the ratio of specific heats are all assumed constant. The construction of this model really assumes that input mass flow rates and, therefore, the output total mass flow rate remain constant in succeeding Δt intervals. Furthermore, the model assumes that in steady state, the vessel accrues no molecules; namely, the inflow of reagents equals the outflow of chemical products. This condition is only approached after 5 to 7 s following the ignition of the combustor. (Lasing begins about 5.5 s after ignition). The reason is that key reagent flows of NF_3 and D_2 must build up and are observed to asymptotically approach a true steady state in an exponential manner. Beyond this point in the actual laser, increases in pressure, P_0, reflect mainly the result of thermal effects in the gas and the vessel. Then from the choked flow equation of one-dimensional gas dynamics[2] the combustor pressure, P_0, changes because of two effects: the square-root dependence on the stagnation temperature, T_0, and more importantly, the inverse dependence on the throat area $A*$.

$$P_0 = C\sqrt{T_0}/A*, \text{ where constant } C = mdot \bigg/ \sqrt{\gamma W \bigg/ R_0 \left(\frac{2}{\gamma+1}\right)^{\frac{\gamma+1}{\gamma-1}}}, \qquad (8)$$

where mdot is the total mass flow rate out of the vessel, γ is the ratio of specific heats, W is the molecular weight after combustion, and R_0 is the universal gas constant. Properties W, g, and c_p require calculations combining the individual properties taken at the gas stagnation temperature, T_e, of the product species according to their mole fractions. For example:

$$W = [cW_{He} + 0.5bW_{N_2} + 2aW_{DF} + \alpha(3b-2a)W_F + 0.5(1-\alpha)(3b-2a)W_{F2}]ndot_{in}/ndot_{out}, \qquad (9)$$

assuming full dissociation into F. Because the consistent combustor solution requires solving for T_o, an iteration on properties must once again be performed to determine T_o. In differential fractional terms for rate of change in the parameters, Eq. (8) becomes

$$dP_o/P_o = -dA*/A* + 0.5\, dT_o/T_o. \tag{10}$$

From Eq. (10), one sees a direct relationship between a thermal gasdynamic parameter, P_o, and a structural or mechanical parameter, $A*$, the throat area, which will be affected by thermal changes. We develop a second equation below to eliminate the fractional change in T_o (for the moment) such that a fractional change in P_o defines a fractional change in $A*$, and, therefore, the thermal condition of the rings in the vessel per unit time, from which $Qdot_{rings}$ can be derived.

In the Alpha Laser, $A*$ represents 25 primary nozzle throats plus two "half" nozzles on the ends of the ring stack. From Figure 2, we model one of the throats as $\varepsilon \cdot c$, where c is the circumference of the ring, r is the radius, and ε is the slit width. Due to thermal effects, both may change dimensionally with time:

$$A* = n\varepsilon \cdot c = n\varepsilon \cdot 2\pi r, \quad n = 26 \text{ throats}. \tag{11}$$

This analysis is helped by the fact that there is absolutely no thermal expansion allowed in the direction of the gain generator cylinder's axis, the z-direction, due to clamping referenced to massive invar rods of the Alpha Laser structure, as shown in Figure 2b.
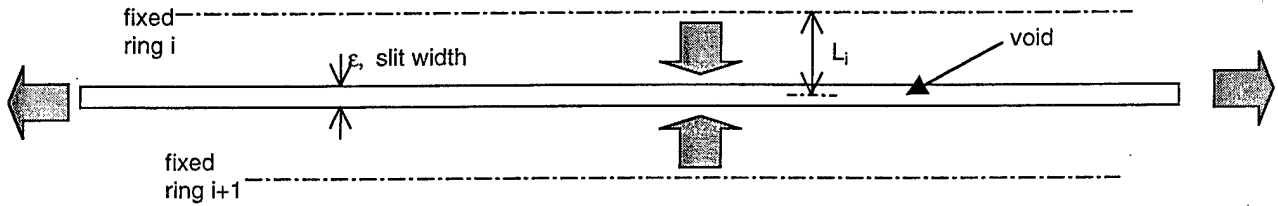

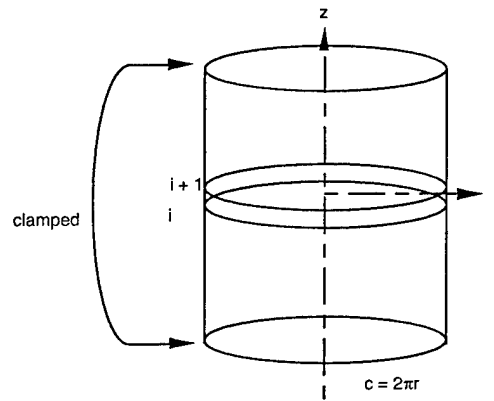Figure 2a. Model of a nozzle throat with length $c = 2\pi r$.

Figure 2b. Concept of gain generator with clamped rings.

10

Due to the clamping condition, the change in area of A* depends only on the thermal expansion of the half section of the ring cross section bordering a particular nozzle, and if one assumes all the expansions are identical for each of the 26 nozzles, $dA^* = n \bullet 2\pi r \bullet d\varepsilon + n \bullet \varepsilon \bullet 2\pi \, dr$.

Between the rigid centerlines in Figure 2a, any shrinkage in ε is due to thermal expansion of the two material half-lengths L_i. (Note L_i is <u>not</u> the geometric half length): $d\varepsilon = -2dL_i$, and it follows that

$$dA^*/A^* = -2 \, [(dL_i/L_i) \bullet (L_i/\varepsilon)] + dr/r. \tag{12}$$

It can be shown that L_i/ε, taken constant in our calculations, is a very slowly varying function of time t, on the order of 2% increase during a typical test. (See Appendix B: Calculation of L/ε.) The thermal linkage is through the coefficient of thermal expansion, CTE, to find an average temperature increase in combustor vessel rings:

$$dL_i/L_i = CTE \bullet \Delta T_{vessel}. \tag{13}$$

Using the perfect gas law to describe the combustor gases yields another relationship for dP_o/P_o. With this additional relationship, T_o and r can be eliminated with Eqs. (10) and (12) to yield the sought relationship, deduction of the temperature change in the material based on merely the change in the combustor plenum pressure:

$$\Delta T\text{-GGA} = (\Delta P_o/P_o) \div [4 \bullet CTE \bullet (L_i/\varepsilon)] \tag{14}$$

The estimation of the heat transfer out of the hot combustor gases to the cylindrical walls of the vessel depends on accurate knowledge of the mass of a gain generator ring. (See Appendix A: Mass Data.) Assuming the convective heat transfer process at the boundary of the end caps is the same, one also needs a knowledge of the mass of the end caps (i.e., the domes) of the vessel. The ring mass is self cooled or regeneratively cooled by the incoming cold reagents. In the Alpha Laser, the end caps are water cooled, providing a slight enhancement of heat transfer out the end domes.

There is a detail in handling the end domes heat transfer. As noted in Appendix A, the end-domes mass has been taken as 15% of the mass of the rings. The idea that the end domes bound both an active annular convective flow region and a stagnating core has been included. Because the domes are water cooled, an additional multiplicative correction, f, to Eq. 16 is

$$f = \left\{ 1 + 0.15 \bullet [(T_{Al} - T_{water})/(T_e - T_{water})] \right\}/1.15, \tag{15}$$

with T_{Al} as the ring temperature at the given time interval, Δt. Generally, T_{water} equals 300K.

The heat transfer rate Qdot (watts) to all parts of the aluminum vessel then is given globally by

$$Qdot_{Al} = M_{Al} \bullet C_{p-Al} \bullet \Delta T_{Al} \bullet f/\Delta t, \tag{16}$$

with the vessel mass being given by M_{Al}, the specific heat of aluminum C_{p-Al}, ΔT_{Al} by Eq. (13), f by Eq. (14), and the time interval, Δt, of heat transfer for the ΔP_o observed, namely, 1.0 s. The Control Volume approach combined with ideas relating to Eq. (7) link vessel material thermal growth to the combustor gas loss:

$$Qdot_{Al} \equiv Qdot_{gas\ loss} \tag{17}$$

6. Calculation of the Stagnation Temperature T_e

Finally, by the heat flux balance of Eq. (2), gas stagnation temperature, T_e, in the combustor is

$$T_e \equiv (Qdot_{inflow} + Qdot_{thermochemical} - Qdot_{gas\ loss}) / (mdot \times c_{p\text{-}gas}), \tag{18}$$

where mdot is the measured mass flow rate of products from the combustor and $c_{p\text{-}gas}$ is the specific heat at constant pressure of products computed according to accurate thermochemical data and mole fractions defined by products (e.g. Eq. 9). Gas properties are computed at T_e. $Qdot_{inflow}$ is the heat flux into the Control Volume due to heat capacity of reagents. $Qdot_{thermochemical}$ is the heat flux added to the flow as products after complete combustion. Because the gas properties of products are computed at T_e, iterations are also needed here to arrive at a consistent solution for T_e, including combustor degree of dissociation effects.

In fact, it should be realized that this stagnation temperature is really a mythical "average" exactly defined by Eq. (18) within the context of one-dimensional gasdynamics analysis. The real gas condition is non-uniform. A differential fluid volume may experience a temperature up to a hypothetical "maximum" combustor temperature (sometimes called T_i) that could be computed without the "gas loss" heat flux term, but adding the heat flux of the reagents used in regenerative cooling. In such a simple model, we view T_e as an average "one-dimensional" stagnation temperature of the gas flowed through the nozzles into the laser cavity.

13

7. Estimation of F-Atom Production

For the given time interval, Δt, once T_e is found, the estimation of F-atoms and molecular F_2 in the combustor follows conventional equilibrium chemistry calculations with T_e as the defined flow "equilibrium" temperature. Inside the combustor, it is assumed that flow effects are negligible and there is sufficient dwell time for the mixture to equilibrate chemically. It has to be confirmed that there are no major bulk fluid dynamical recombination effects to generate F_2 through the nozzles. Indeed, there is a minor correction of flows from the combustor to the nozzle throat because fluid particle times are sufficiently long to allow some recombination. However, from the throat to the exit, the flow becomes on the average hypersonic, and any effects can be shown to be negligible (Appendix C). It can be shown that loss of F-atoms by wall and boundary layer recombination effects is negligible for this nozzle design, based on wall data discussed by N. Cohen et al.[6] Thus, the principal loss of F-atoms is presumed to occur by three-body bulk recombination in the presence of diluents and other exhaust products.

The dissociation of F_2 into F-atoms in this model is given by

$$k_f = 5 \times 10^{13}\, \sigma \exp[-35,000/R_o T_e],\ (cm^3\text{-mole}^{-1}\text{-s}^{-1}),\tag{19}$$

$\sigma = 1$ for all collision partners except He, $\sigma = 2$, F_2 itself, $\sigma = 2.7$, and F-atoms, $\sigma = 10$. The specific reference is N. Cohen and J. F. Bott.[7] Instead of the more commonly JANAF-accepted bond strength of 38 kcal-mole^{-1}, we have used 35 kcal-mole^{-1} as recommended by Cohen. The backward rate coefficient for this model is fitted to the early data summary[6]

$$k_b \approx (2.6 \times 10^{16})/T_e^{1.05},\ (cm^6\text{-mole}^{-2}\ s^{-1})\tag{20}$$

and the equilibrium constant K is simply k_f/k_b. The maximum number of F-atoms (i.e., the F-atom density $[F_o]$) available in the combustor can be computed following Eq. (4) with unity degree of dissociation and for very high T_e, given the gas properties of the gas. For the 1-s interval of apparent steady state, this is equivalent to the flowrate of F atoms that will leave the plenum as well. However, the actual number of F-atoms in the combustor that makes up the desired F-atom flow rate depends on T_e. The solution for the actual F-atom density [F] is quadratic, for the positive branch

$$[F] = 0.25 \cdot K\left\{-1 + \sqrt{1 + 8F_o/K}\right\}\tag{21}$$

It follows that in the given local fluid particle, density $[F_2]$ and degree of dissociation, α, are

$$[F_2] = 0.5\ \{[F_0] - [F]\}\tag{22}$$

$$\alpha = \left\{ 1 + 2 \bullet ([F_2]/[F]) \right\}^{-1} \tag{23}$$

The admittedly large uncertainty in the activation energy of Eq. (19) and the empirical curve fit in Eq. (20) mean the uncertainties in the estimations of F-atom and F_2 densities will remain high except in the vicinity of unity α. Model uncertainties will be discussed further below. The efficient HF continuous-wave chemical laser usually requires the suppression of F_2 species. This is achieved by ensuring sufficiently high T_e, in the combustor. For a space system, a requirement for high T_e must be traded against the mass increase in reagents for producing the hotter gain generator.

8. Model Results and Discussion

The model is demonstrated using recent Alpha Laser input test data from Tests HL902[1] and HL909B[8]. We caution at the onset that the model prediction of degree of dissociation α or of F-atom flow rate will remain unverified, for there are no independent direct experimental measurements. Nevertheless, certain observed behaviors of laser power as a function of time in HL902 and HL909B are consistent with model findings. Table 1 summarizes the flow condition for HL909B when the reagents have reached a near steady state at the onset of lasing (t = 8 s) In reality, both NF_3 and D_2 increase 1% or less during the time of lasing. Flow conditions are similar for HL902.

The key test observable is the measured combustor plenum pressure as a function of time from zero seconds to reagents shutoff. In the Alpha Laser test series, data are taken at 0.25-s intervals. This work will use data only at each 1.0-s interval for most of our cases because the rate of change of the pressure in this interval is sufficiently small, typically 5% or less. The estimated errors on this measurement are 3% or less.

From the HL909B combustor pressure P_c as a function of time, one can deduce the apparent heat loss to the vessel for each 1-s block of the study. From the computed heat fluxes for a given t, Δt block (Eqs. 3, 6, 16, 17), one can deduce the probable T_e based on Eq. (18). This parameter is found to have a considerable range as a function of time, from 1423K to 1563K in this computation during lasing, from t = 9 s to t = 15 s. This spread is reflected in the computations for degree of dissociation α, as exhibited in Figure 3. (diamonds)

Table 1. HL909B Combustor Flow Conditions Used in the Model (t = 8 s)

	Parameter	Comments
NF_3 Flowrate, mol/s	112.9	Entry at 300K
D_2 Flowrate, mol/s	111.5	Entry at 80K
He Flowrate, mol/s	573.5	Entry at 100K, taken as 80K
Reagents Molecular Weight, g/mol	13.50	
Reagents Specific Heat c_p, J/g-K	1.928	
Reagents Sp. Heat Ratio, γ	1.470	
Combustion Products		Complete reaction assumed
Product: max-F (or F_0), mole/s	117.2	No recombination or loss
Product: N_2, mole/s	56.44	
Product: DF, mole/s	221.4	
Product Molecular Weight, g/mol	11.11	
Product Specific Heat, c_p, J/g-K	2.082	
$MdotF_0/A$, kg/m^2	0.330	
Product Sp. Heat Ratio, γ	1.561	

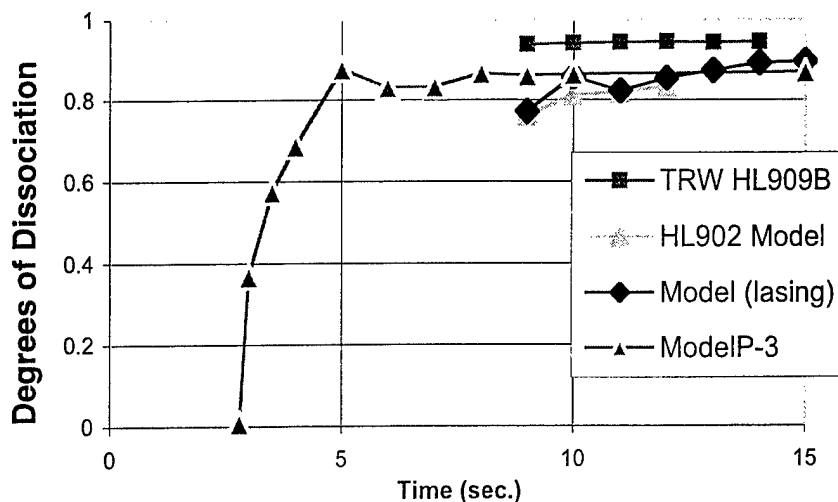## Calculation of HL909B Degree of Dissociation

Figure 3. Model estimation of degree of dissociation for test HL909B.

The degree of dissociation or α curve labeled "Model (lasing)," from 9 to 15 s, exhibits an approach to "steady state" for times greater than 10 s, with α approaching 0.90. Here, the Pc and reagent flow rate data are taken from test data1,8 from HL909B. Since data used are in 1-s intervals of time, high-frequency temporal details are disregarded in this model.

Comparison of HL902 degree of dissociation results can be made with those of HL909B. The model can be run with HL902 pressure and flow conditions, which are very similar. HL902 α's (grey triangles, labeled "HL902 Model") are slightly lower than those of HL909B, but within 5%. The good agreement is confirmation of the contention that test reagent flow rates have been the same for at least 10 tests in the series, spanning HL902 to HL909B. Comparison can also be made with a contractor model (squares, labeled "TRW HL909B")8 based on a similar heat flux balance approach, which uses data from embedded thermocouples in the rings. The TRW model seems to predict higher α at earlier times averaged over a much more steady state, possibly an indication of insensitivity of the thermocouples to more rapid changes in gas flow conditions. The thermocouples are highly sensitive to vessel thermal non-uniformities and the quality of their placements. The trend toward agreement in degree of dissociation (within 10%) of two model approaches at late times past 10 s. suggests progress toward prediction of this elusive key parameter.

We have included a fourth computation (Model P-3)9,10, which attempts to synthesize the transient degree of dissociation in HL909B toward steady state in the case of both pressure and thermal transient changes. As we suggested earlier, both the current and the advanced models converge to the same dissociation results as flows reach a steady state, at $t \geq 8-10$ s.

18

The absence of direct measurements for F-atoms or α at the nozzle array exit plane makes model validation difficult. We must resort to plausibility discussions that demonstrate the model's consistency with other observed data. We examined three types of data:

1. Typical thermocouple data for the rings

2. Spectra behavior as a function of time beyond 11 s

3. P(t), outcoupled power as a function of time, seen to be slowly increasing

In all cases, the model seems to provide insight into data variations or demonstrate consistency.

In the Alpha Laser, thermocouples were mounted manually in various gain generator ring positions. Although the absolute values had considerable scatter, they seemed to exhibit time constants longer than a fraction of a second, and a common trend appeared to be an average temperature increase of 15K/s over most of the running time. The model prediction from Eq. (14) is shown in Figure 4, together with a comparison to a 15K/s slope line. It can be seen that there is qualitative, even quantitative agreement over a wide span of time.

The observation of spectra at times greater than approximately 11 s in a lasing test can be seen from the data of relative laser power as a function of time, as in Figure 5. The framed region corresponds to a lasing time region when α has not reached a steady state. For times greater than around 10.5 s, it can be seen that most spectral lines are steadier as a function of time.

The best demonstration of an approach to steadiness is P2(6) and P2(7) while P1(7) declines slightly. Steady spectral signals are an indication that laser power has attained a steady condition. In turn, this implies proportionally that the F-atom flowrate and therefore α has become constant for longer times,
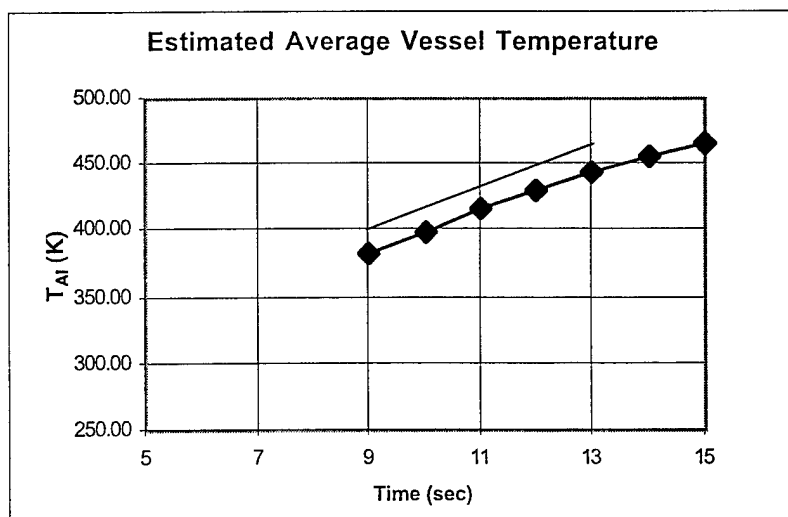

Figure 4.   Growth in ring temperature computed by the model. The line delineates 15K/s.
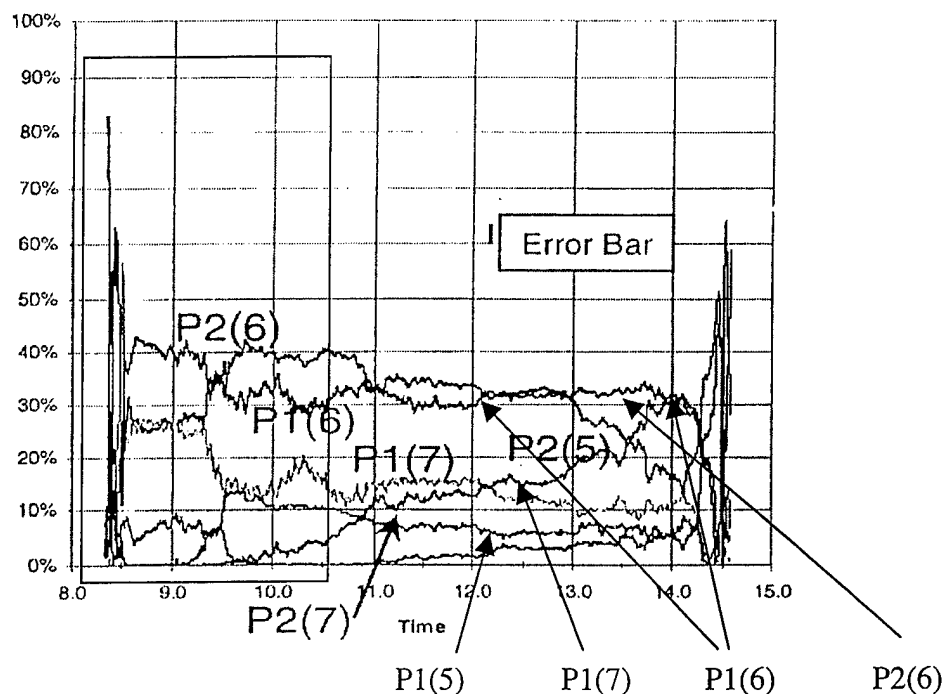
Figure 5. Outcoupled laser power spectra for times greater than 11 s.
HL909B.

as forecast by our model. The increases as a function of time in P1(5) and P2(5) have also been correctly attributed to gain generator thermal ring growth. Ring growth pushes the gain width outward to better couple with the mode width of the resonator and away from the obstruction caused by protective clippers at the nozzle exit plane.8 Likely both effects, α growth and ring growth, are present. Lower J lasing lines such as J = 5 are more sensitive to this thermal growth because of the sharper peaked spatial distributions of the low J small-signal gains upstream in the medium. However, for HL909B, P1(6) experiences an anomalous "dip" at 13.5 s before recovering. Thus, in fact, HL909B data are not as convincing a validation as some earlier spectral data, such as HL909A,8 in showing steadier power as α approaches a steady value at long operating times.

The third check is on observed laser power as a function of time, P(t), as shown in Table 2. In this table, the reported outcoupled laser power from test HL909B is normalized to its maximum observed value, between 12 and 14 s. To a zeroth-order-level approximation, we assume that the laser power extracted must be proportional to the F-atom flow into the resonator, and therefore degree of dissociation, normalized to our computed quantity, at 14 s.

This normalization can be compared with the actual similar trend in normalized data to suggest that the slight empirical increase in laser power as function of time, P(t), might be due partly to the slow increase to steady state of parameter α. As noted earlier, ring growth also contributes to P(t) increase, and may be the reason for the larger part of the P(t) increase after 10 s. Nevertheless the time-dependent pressure curve, Pc, plus slight temporal increase in reagent flows generate a performance prediction from our model consistent with an observed power trend.

20

Table 2. Comparison of Adjusted Model to Normalized HL909B Outcoupled Power8

Time (s)	Normalized _	HL909B
9	0.86	0.71
10	0.96	0.87
11	0.92	0.96
12	0.96	1.00
13	0.98	1.02
14	1.00	1.00

Outcoupled powers are normalized to values at t = 14 s.

The general trends exhibited by the three empirical checks suggest that the model is consistent with observations. However, verification remains inconclusive without more data and experiments.

9. Model Uncertainty

The exponential structure of the equations for F-atom density, Eqs. 19–20 combined, suggest that any calculation of that parameter using empirical data will be subjected to accumulating errors in the F_2 to F density ratio in Eq. (23). If one supposes that the ratio of densities of F_2 to F-atoms can be established to the reasonable uncertainty of ±20%, then the fractional uncertainty, $\Delta\alpha/\alpha$, can be shown to depend on the value of α as in Figure 6. The uncertainty is computed assuming a root-sum-square fractional error dependence for independent error sources in experiments that are not repeated.

For example, the uncertainty in estimating $\alpha = 0.9$ is ±2.5%. On the other hand, if α is computed to be 0.4, the uncertainty is ±12%. The uncertainty in knowing α approaches the uncertainty in establishing the F_2/F density ratio for very small values of α. For any value of α, the density of F_2 is difficult to establish even though the total number of F-atoms can be easily computed from thermochemical calculations. There is obviously less uncertainty in this density as α approaches unity; thus, it is clear that the model is most useful for degrees of dissociation approaching unity.
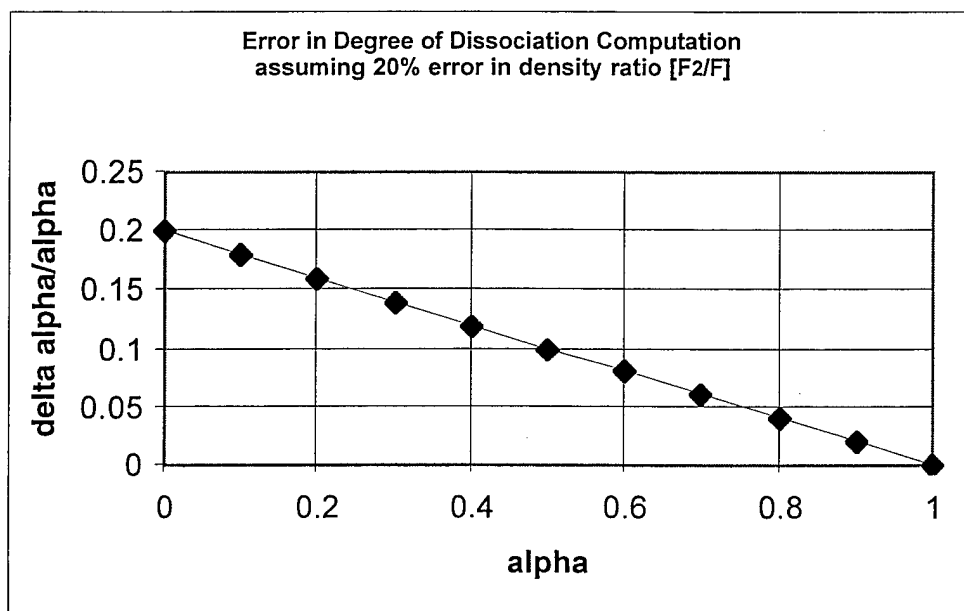
Figure 6. The uncertainty in computing degree of dissociation, α.

10. Closure

In reality, accuracy limitations of experimental laser data and the chemical kinetic database, especially the high sensitivity of equilibrium constant K to small uncertainties, may make it futile to strive for high accuracy in the density ratio. Then the utility of such models for detailed design is necessarily limited. We contend that such models are important, perhaps even invaluable, tools for guidance and insight, but may not be very useful for detailed design or planning except when combustor temperatures are set sufficiently high, with the degree of fluorine dissociation nearing unity.

The reader is cautioned that although this model is approximately correct as the combustor approaches "steady state," subsequent work generated a better formulation to handle the large unsteadiness in flow parameters at the onset of ignition and the approach to this quasi-steady-state condition. It was also later found that the combustor stagnation pressure, P_c, could not be successfully modeled as a function of time without developing the concept of a colder inner cylindrical core in this model. These adjustments are contained in the latest and final versions of the model.

Appendix A—Mass Data for the Alpha Gain Generator

The following mass data was acquired from the Alpha Laser Optimization program.

Normal Ring	11.6 kg
End Ring	11.0 kg
Sub assemblies per ring	0.85 kg
Domes	1.15 kg

PRECEDING PAGE BLANK

Appendix B—Calculation of L/ε as a Function of Run Time

In a somewhat circular argument, we assume L/ε is nearly constant, with $L = L_o = 18.2$ mm and $\varepsilon = \varepsilon_o$ = 0.6634 mm defined by the system geometry. By Eq. (14), we can estimate ΔT-GGA. Using this temperature, we can estimate the increase in L (Eq. 13) and the decrease in ε (Eq.12) as a function of time.

t (s)	po (psia)	Δt (1 s)	Δpo/po=?	ΔT-GGA	ε (mm)	L (mm)	L/ε
4	30				0.6638	18.20	27.42
5	32.8	4 to 5	0.0933	37.0	0.6621	18.22	27.51
6	36.1	5 to 6	0.1006	39.9	0.6603	18.23	27.61
7	37.7	6 to 7	0.0443	17.6	0.6595	18.24	27.66
8	39.8	7 to 8	0.0557	22.1	0.6584	18.25	27.72
9	41.7	8 to 9	0.0477	18.9	0.6576	18.26	27.76
10	43.5	9 to 10	0.0432	17.1	0.6568	18.26	27.81
11	45.5	10 to 11	0.0460	18.2	0.6559	18.27	27.86
12	47.1	11 to 12	0.0352	13.9	0.6553	18.28	27.89
13	48.9	12 to 13	0.0382	15.2	0.6546	18.28	27.93
14	50	13 to 14	0.0225	8.9	0.6542	18.29	27.95
15	51	14 to 15	0.0200	7.9	0.6538	18.29	27.98

From t = 4 s to t = 15 s, L/ε increases only around 2%, thus validating our assumption that L/ε is nearly constant.

We have noted through References 9 and 10 that estimating ΔT-GGA by this method for early times may not be exactly correct because time-dependent changes in p_o may depend on flow variations as well as the thermal effects of this model.

PRECEDING PAGE BLANK

Appendix C—Estimate of Volumetric F-Atom Loss from Plenum to Exit

We contended that the volumetric loss in a one-dimensional nozzle flow from plenum to exit of F-Atoms is around 1%. The contour pattern, A/A* for the HYWN nozzle was made available by the contractor. This does not include boundary layer effects. The table below summarizes our result for a high degree of fluorine dissociation in the plenum. Parameter "x" is flow in the radial direction, "A/A*" is the nozzle area expansion, "M" is the Mach number, "T/T_o" is the relative static temperature at station x, "[F]" is the molar concentration of F-atoms (Eqs. 19–21), and "alpha" (Eq. 23) is the degree of dissociation. The ratio of alpha at x = 27.3 mm and x = 0 mm (plenum) shows less than a 1% loss.

x(mm)	A/A*	M	T/T_o	[F]	alpha
0	7.41	0.08	0.9983	1.9371E-06	0.964
1.1	6.48	0.09	0.9978	1.9204E-06	0.962
2.2	4.63	0.12	0.9957	1.9008E-06	0.960
3.3	2.78	0.21	0.9878	1.8652E-06	0.959
4.4	1.57	0.40	0.9571	1.7583E-06	0.958
5.7	1.00	1.00	0.7810	1.2221E-06	0.958
0.0	1.00	1.00	0.7810	1.2217E-06	0.958
1.1	3.45	3.04	0.2790	1.9502E-07	0.958
2.2	3.98	3.23	0.2553	1.6639E-07	0.958
3.4	6.63	3.94	0.1871	9.5607E-08	0.958
4.5	9.54	4.48	0.1507	6.5001E-08	0.958
5.7	10.87	4.69	0.1396	5.671E-08	0.958
6.8	13.25	5.01	0.1243	4.6122E-08	0.958
9.1	16.44	5.38	0.1096	3.6854E-08	0.958
11.4	18.56	5.60	0.1021	3.2509E-08	0.958
13.6	21.21	5.84	0.0946	2.8344E-08	0.958
15.9	23.32	6.02	0.0895	2.5707E-08	0.958
18.2	25.45	6.19	0.0851	2.3487E-08	0.958
20.4	29.16	6.46	0.0787	2.0433E-08	0.958
22.7	30.48	6.55	0.0767	1.9528E-08	0.958
25	32.61	6.69	0.0738	1.8222E-08	0.958
27.3	34.99	6.83	0.0709	1.6966E-08	0.958

In this calculation, we have taken plenum conditions to be T_o = 1858K, p_o = 39.8 psia, γ = 1.56, and W = 11.1 g-mol^{-1} as determined by mole fractions of products (See, for example, Table 1). Initial alpha= 0.964 in the plenum.

References

1. Wiest, T., Norris, J., Amimoto, S., Kwok, M., Novoseller, D., and Bradford, R. S. "Progress in Alpha Laser Characterization," AIAA 99-3545, 30th Plasmadynamics and Lasers Conference, Norfolk, VA. 28 June-1 July 1999, 10 pp.

2. Shapiro, A. H., *The Dynamics and Thermodynamics of Compressible Fluid Flow, Vol I*. The Ronald Press Company, New York, 1953.

3. Stull, D. R. and Prophet, H., Project Directors "JANAF Thermochemical Tables, 2nd Edition, U.S. Dept. of Commerce National Bureau of Standards, NSRDS-NBS 37, June 1971, 1141 pp. Also Chase, Jr., M. W., Curnutt, J. L., Downey, Jr., J. R., McDonald, R. A., Syverud, A. N., Valenzuela, E. A. "JANAF Thermochemical Tables, 1982 Suppl.," *J.Phys.Chem.Ref.Data*, **11**, No. 3, Supplement 1, August 1982, pp 695-940.

4. Chase, Jr., M. W., Davies, C. A., Downey, Jr., J. R., Frurip, D. J., McDonald, R. A., and Syverud, A. N. "JANAF Thermochemical Tables, Third Edition." *J.Phys.Chem.Ref.Data*, **14**, Supplement 1, Parts 1 and 2, (1985) 1855 pp.

5. Ibid. NIST Standard Database 13 or NIST13.

6. Cohen, N. "A Review of Rate Coefficients in the H2-F2 Chemical Laser System-Supplement (1977), SAMSO-TR-78-41, 8 June 1978, pp 7-9.

7. Cohen, N. and Bott, J. F. "A Review of Rate Coefficients in the H_2-F_2 Chemical Laser System," SAMSO-TR-76-82, 15 April, 1976. Pp 10-16.

8. Novoseller, D. "Recent Results From the Alpha Laser Optimization Program," AIAA-2000-2498, 31st Plasmadynamics and Lasers Conference, Denver, CO, 19 June-22 June 2000.

9. Kwok, Munson A. "A Model Predictor for Chemical Laser Combustors," AIAA 2001-2868, 32nd AIAA Plasmadynamics and Lasers Conference, Anaheim, CA. 11-14 June, 2001, 11pp.

10. Kwok, Munson A. "A Model Predictor for Chemical Laser Combustors," Aerospace Corporation Technical Report, TR-2001(1019)-2, 15 December 2001, 11 pp.

PRECEDING PAGE BLANK

LABORATORY OPERATIONS

The Aerospace Corporation functions as an "architect-engineer" for national security programs, specializing in advanced military space systems. The Corporation's Laboratory Operations supports the effective and timely development and operation of national security systems through scientific research and the application of advanced technology. Vital to the success of the Corporation is the technical staff's wide-ranging expertise and its ability to stay abreast of new technological developments and program support issues associated with rapidly evolving space systems. Contributing capabilities are provided by these individual organizations:

Electronics and Photonics Laboratory: Microelectronics, VLSI reliability, failure analysis, solid-state device physics, compound semiconductors, radiation effects, infrared and CCD detector devices, data storage and display technologies; lasers and electro-optics, solid-state laser design, micro-optics, optical communications, and fiber-optic sensors; atomic frequency standards, applied laser spectroscopy, laser chemistry, atmospheric propagation and beam control, LIDAR/LADAR remote sensing; solar cell and array testing and evaluation, battery electrochemistry, battery testing and evaluation.

Space Materials Laboratory: Evaluation and characterizations of new materials and processing techniques: metals, alloys, ceramics, polymers, thin films, and composites; development of advanced deposition processes; nondestructive evaluation, component failure analysis and reliability; structural mechanics, fracture mechanics, and stress corrosion; analysis and evaluation of materials at cryogenic and elevated temperatures; launch vehicle fluid mechanics, heat transfer and flight dynamics; aerothermodynamics; chemical and electric propulsion; environmental chemistry; combustion processes; space environment effects on materials, hardening and vulnerability assessment; contamination, thermal and structural control; lubrication and surface phenomena. Microelectromechanical systems (MEMS) for space applications; laser micromachining; laser-surface physical and chemical interactions; micropropulsion; micro- and nanosatellite mission analysis; intelligent microinstruments for monitoring space and launch system environments.

Space Science Applications Laboratory: Magnetospheric, auroral and cosmic-ray physics, wave-particle interactions, magnetospheric plasma waves; atmospheric and ionospheric physics, density and composition of the upper atmosphere, remote sensing using atmospheric radiation; solar physics, infrared astronomy, infrared signature analysis; infrared surveillance, imaging and remote sensing; multispectral and hyperspectral sensor development; data analysis and algorithm development; applications of multispectral and hyperspectral imagery to defense, civil space, commercial, and environmental missions; effects of solar activity, magnetic storms and nuclear explosions on the Earth's atmosphere, ionosphere and magnetosphere; effects of electromagnetic and particulate radiations on space systems; space instrumentation, design, fabrication and test; environmental chemistry, trace detection; atmospheric chemical reactions, atmospheric optics, light scattering, state-specific chemical reactions, and radiative signatures of missile plumes.